AGU ADVANCING EARTH AND SPACE SCIENCE

Earth and Space Science

RESEARCH ARTICLE
10.1029/2021EA002049

Special Section:
The Arctic: An AGU Joint Special Collection

Summer Marine Fog Distribution in the Chukchi–Beaufort Seas

Li Yi[1], King-Fai Li[2], Xianyao Chen[1], and Ka-Kit Tung[3]

[1]Frontiers Science Center for Deep Ocean Multispheres and Earth System, Key Laboratory of Physical Oceanography, Ocean University of China, Qingdao, China, [2]Department of Environmental Sciences, University of California, Riverside, CA, USA, [3]Department of Applied Mathematics, University of Washington, Seattle, WA, USA

Key Points:

- Pacific Arctic marine fog occurrence frequency are derived using ship-based and satellite-based measurements
- Ship-based marine fog occurrence in the early morning is two times more frequent than that in the evening
- Longitude-latitude fog frequency distribution is linked to Pacific warm flow and its interaction with Arctic cold front

Supporting Information:

Supporting Information may be found in the online version of this article.

Correspondence to:
K.-F. Li,
king-fai.li@ucr.edu

Citation:
Yi, L., Li, K.-F., Chen, X., & Tung, K.-K. (2023). Summer marine fog distribution in the Chukchi–Beaufort Seas. *Earth and Space Science*, *10*, e2021EA002049. https://doi.org/10.1029/2021EA002049

Received 2 OCT 2021
Accepted 25 JAN 2023

Author Contributions:
Conceptualization: Li Yi, King-Fai Li, Ka-Kit Tung
Funding acquisition: Xianyao Chen
Investigation: Li Yi, King-Fai Li, Xianyao Chen
Methodology: Li Yi, King-Fai Li, Ka-Kit Tung

Abstract We study the spatial and temporal variability of summer marine fog in the Chukchi–Beaufort region (175°E−150°W, 70°–86°N) using the in-situ visibility measurements aboard the Chinese research fleet Xuelong (I and II) and a fog product we derive using the Vertical Feature Mask product of the spaceborne Cloud-Aerosol Lidar and Infrared Pathfinder Satellite Observation (CALIPSO) observations. The Xuelong in-situ observations show that the fog frequency in the Chukchi–Beaufort region has a maximum of ∼18% in the early morning and is less than 10% in the rest of the day. The latitudinal distribution of the Xuelong-based in-situ fog frequency further shows high fog occurrences at 74°N and 79°N, which are related to the local high fog occurrences near 72°–74°N and 76°–80°N in the central Chukchi–Beaufort region, as revealed by the longitude-latitude pattern of the CALIPSO-based spaceborne fog frequency distribution. The CALIPSO-based fog frequency is also shown to be lower along the continental coastlines than in the Chukchi–Beaufort region. This longitude-latitude distribution may be explained by a reduced fog formation due to the Pacific warm current flowing into the Arctic region through the Bering Strait in the summer as well as an enhanced fog formation in the Chukchi–Beaufort region when the southward flow of the Beaufort Gyre interacts with the Pacific warm current.

1. Introduction

While the abrupt shrinking of summer Arctic sea ice extent may adversely accelerate global change, it ironically also brings unexpected economic growth to the otherwise inaccessible Arctic Sea regions. Climate models project that the first ice-free Arctic summer could happen in as early as the 2030s (Snape & Forster, 2014). Smith and Stephenson (2013) estimated that by the middle of this century, the much reduced sea ice will allow open-water ships to cross the Arctic along the Northern Sea Route in September. As a result, the typical cost of using the traditional shipping route of going between the western Pacific and Europe via the Suez Canal may be reduced by more than 50% by using the Northern Sea route through the Arctic instead. However, a potential safety issue is the marine fog over the new open-water regions due to heat and moisture exchange between ocean and atmosphere (Eastman & Warren, 2010; Intrieri et al., 2002; Kay & Gettelman, 2009; Palm et al., 2010; Schweiger et al., 2008; Wang & Key, 2005), especially during the summertime when most trans-Arctic traffic is expected (Naval Weather Service, 1978; Venne et al., 1997). Besides marine traffic, aircrafts under low visibility condition due to the presence of marine fog are also required to fly with instrument flight rules to reduce the chance of human errors.

Observations of global marine fog, such as those compiled in the International Comprehensive Ocean-Atmosphere Data Set (ICOADS), have been primarily based on in-situ weather reports directly made aboard commercial ships and research vessels. However, these observations are mainly limited to regions from ∼30°S to ∼75°N; data over the polar regions are very rare, except for some ship tracks near the Arctic coastlines. Considering all available data from 1950 to 2007, Dorman et al. (2017) showed that marine fog forms most frequently in the summer (June–July–August, or abbreviated as JJA) east of mid-latitude coasts such as the seas in the northwest Atlantic near Newfoundland and the Sea of Okhotsk in the northwest Pacific. The marine fog frequencies, defined as the number of reported fogs at a grid point divided by the total number of reports at the same grid point, in those high-fog areas during the summer are generally higher than 40% and may be as high as 60% in the Sea of Okhotsk. These values are at least two orders of magnitude higher than the global annual median, which is only 0.2%. Marine fog is expected to form more frequently over the Arctic Sea than at lower latitudes due to advection fog (when warm moist air moves over cooler sea surface) and steam fog (when cold air passes over warmer water) (Koračin et al., 2014). However, the latitudinally limited ICOADS data hinders a comprehensive characterization of the distribution of Arctic marine fog. Shupe et al. (2011) studied the occurrence of all cloud types, including

Project Administration: Xianyao Chen, Ka-Kit Tung
Supervision: Xianyao Chen, Ka-Kit Tung
Writing – original draft: Li Yi, King-Fai Li
Writing – review & editing: Li Yi, King-Fai Li

those with cloud base lower than 2 km, in the western Arctic based on the lidar measurements of cloud-top and cloud-base heights at 5 ground observatories and a 1-year-long ship-based observatory (Surface Heat Budget of the Arctic (SHEBA), Uttal et al., 2002), but there has not been any long-term study tailored for Arctic marine fog based on visibility measurements.

Recently, the Chinese polar research fleet, Xuelong (literally meaning "Snow Dragon"), conducted 3 scientific expeditions in the Arctic region from 2016 to 2018 (by Xuelong I) and 1 scientific expedition in 2020 (by Xuelong II), which included in-situ visibility observations en route. Their visibility observations provided some rare data for assessing fog occurrences in the Arctic for the first time and supplemented the ICOADS database. In this work, we will derive a distribution of marine fog in the Chukchi–Beaufort Seas north of Alaska using the in-situ weather reports made aboard Xuelong. The visibility-based marine fog distribution to be obtained will be the first of its kind in the Pacific Arctic region.

However, in-situ observations like those obtained aboard Xuelong are limited in both space and time. Operational monitoring of marine fog based on satellite measurements is a promising complement to ground observations, but it requires a remote sensing technique able to resolve cloud layers in the first few hundred meters above the surface. Yi et al. (2019) deploys an infrared-based method to detect cloud layers with a cloud-base below 300 m, but the vertical resolution of infrared measurements (greater than a few hundred m) cannot further distinguish surface-touching fog from stratus clouds hanging above surface; their method also requires external information of the sea surface temperature (e.g., those from reanalyses) beneath the cloud layer to infer the cloud-base height. In contrast, the lidar-based instrument aboard the National Aeronautics and Space Administration (NASA)'s Cloud-Aerosol Lidar and Infrared Pathfinder Satellite Observation (CALIPSO) has a much higher vertical resolution of ∼60 m and is able to directly measure the cloud-base height of a moderately thick cloud (with an optical depth less than 3). Wu et al. (2015) demonstrated the potential of using CALIPSO to detect surface-touching fog over the Yellow Sea in Northwest Pacific. We expect that the same technique should be applicable to the Arctic. Thus, in addition to the in-situ fog distribution, we will derive another distribution of Arctic marine fog in the same region using CALIPSO measurements.

2. Data and Methods

2.1. The Xuelong Expeditions

We will use the fog observations made at the surface of the Arctic Ocean during the Xuelong expeditions. Xuelong I and II are icebreaking research vessels with displacements of 21,000 and 14,000 ton respectively. Figure 1 shows the four expeditions in the summers of 2016, 2017, 2018, and 2020 to be used in this study: the red line was the route from 25 July 2016 to 2 September 2016; the pink line was the route from 31 July 2017 to 21 September 2017; the blue line was the route from 30 July 2018 to 6 September 2018 and the green line was from 27 July 2020 to 12 September 2020.

Xuelong I acquired the visibility en route using the sensor CAMPBELL CS120, which uses infrared (at 850 nm) forward-scatter technology to estimate the local visibility under the sensor (https://s.campbellsci.com/documents/us/product-brochures/b_cs120.pdf). The measured visibility ranges from 12 m to 32 km. The accuracies are ∼10% and ∼20% for visibility below 10 km and between 10 and 20 km, respectively.

Simiarly, Xuelong II acquired the visibility en route using Vaisala PWD22, which uses infrared (at 875 nm) forward-scatter technology to estimate the local visibility under the sensor (https://fluidic-ltd.co.uk/?ddownload=12120). The measured visibility ranges from 10 m to 20 km. The accuracies are ∼10% and ∼15% for visibility below 10 km and between 10 and 20 km, respectively.

Both detectors sample the visibility every 1 min. For these 1-min intervals, we follow World Meteorological Organization (WMO)'s definition to define a fog event if the measured visibility is less than 1 km (WMO, 2005). However, sea spray formation due to the wind shear and ocean wave breaking under high winds may also result in low visibility. Andreas (2004) suggests that the sea spray flux is ∼10% of the total air–sea momentum flux when the wind speed at 10 m is 11–13 m s^{-1} (or approximately 21–25 knots). To minimize the sea spray events in our detected fog events, we exclude raw records where both the 1- and 10-min wind speeds measured by Xuelong were greater than 13.375 m s^{-1}. In addition, the recorded relative humidity of all fog events identified in the Xuelong records were greater than 80%. So we do not apply any screening on the relative humidity.

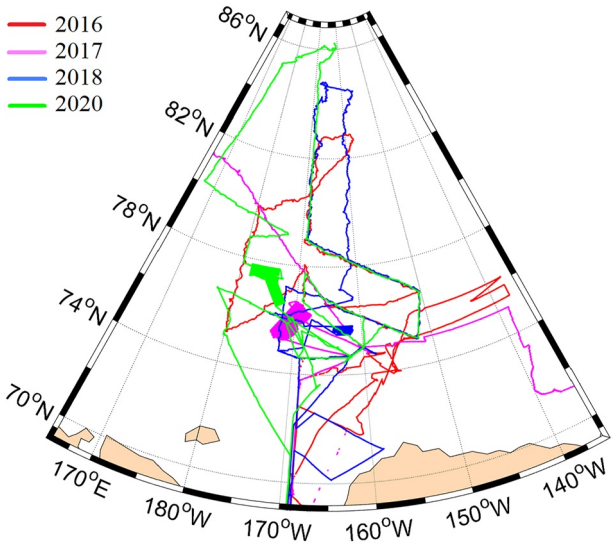

Figure 1. The tracks of Xuelong I and II over the Chukchi–Beaufort seas in 2016 (red), 2017 (pink), 2018 (blue), and 2020 (green).

Since a fog layer may last longer than the 1-min sampling interval, direct use of the raw 1-min visibility records may result in an apparent oversampling of the same fog event many times while they are falsely treated as independent events. To reduce the statistical degrees of freedom, we thus repartition Xuelong's 1-min visibility record into 15-min segments and define a 15-min segment as a fog event if at least 8 min within the segment had visibility less than 1 km. This effectively reduces the degrees of freedom to ∼4 in a 1-hr window. Our choice of the 15-min partitioning is similar that of SHEBA (10 min) used in Shupe et al. (2011). In all subsequent analyses, we study the fog occurrence using the 15-min segments instead of the raw 1-min records.

2.2. CALIPSO VFM Products

The CALIPSO Level 2 product set (L2_VFM-Standard-V4-20; https://www-calipso.larc.nasa.gov/resources/calipso_users_guide/data_summaries/vfm/index_v420.php) is used in this study (Mülmenstädt et al., 2018; Winker et al., 2009). The lidar measurements to be used in this study are provided by the Cloud-Aerosol Lidar with Orthogonal Polarization (CALIOP) instrument. Variables to be used in fog detection include the track time (code name: Profile_UTC_Time), geolocation information (longitude and latitude), surface type (Land_Water_Mask for shallow ocean, land, coastlines, shallow inland water, intermittent water, deep inland water, continental ocean, deep ocean) and VFM (Feature_Classification_Flags). The "Feature Type Field" in the VFM product specifies "invalid" (bad or missing data), "clear air," "cloud," "aerosol," "stratospheric feature," "surface," and "no signal." The "Feature Type Quality Assessment" specifies whether the retrieved feature type is of "no confidence," "low confidence," "medium confidence," or "high confidence." The VFM product spans from −0.5 km (negative sign means below sea level) to 30 km, at 30-m intervals below 8.2 km. The ground layer spans from −20 to 10 m.

The sun-synchronous orbit of CALIPSO surveys latitudes between 82°S and 82°N twice daily. Unlike the fixed crossing times ∼1:30 a.m./p.m. at low latitudes (≤∼60°), CALIPSO crosses the Arctic region at rapidly changing local times from ∼3 a.m. (descending) or ∼12 p.m. (ascending) at 70°N to 7:30 a.m. only (orbital node) at 82°N. CALIPSO repeats its orbital scan on the same 172-km (or 1.55°-longitude) grid at the equator every 16 days. CALIOP has a footprint of 70 m and it scans across the track every 333 m along the track (Winker et al., 2007).

At each sub-satellite point, we search for the first cloud layer starting from the ground. The bottom altitude of the first cloud layer is defined as the cloud base height. If the bottom cloud layer is in the first CALIPSO level at −20 m (i.e., the lowest CALIPSO 30-m layer containing ground and topped at 10 m above ground), then we define this observed cloud layer as fog. Note that we do not apply the WMO definition of fog based on horizontal visibility when processing CALIPSO measurements.

2.3. The Study Region in the Chukchi–Beaufort Seas

All Xuelong Expeditions entered the Arctic region from the Bering Strait. Xuelong spent most of its time in the Chukchi–Beaufort seas, except in 2017, when it surveyed around the Arctic along the coastlines of Canada and Greenland. Therefore, most of the reported fog events were in the Chukchi–Beaufort seas. To define an appropriate area for the comparison between Xuelong's observations and CALIPSO fog detection, we focus on the area defined by longitudes from 176°E to 152°W and latitudes from 70° to 86°N (the maximum latitude Xuelong reached).

2.4. Validation

It is necessary to validate collocated Xuelong and CALIPSO observations to ensure the accuracy of our satellite-based fog detection algorithm. Given that the swath width of CALIPSO is only 333 m, finding footprints that overlap with Xuelong's position is challenging. We found 6 collocated events in the summers of 2016,

Table 1
Collocated Xuelong and Cloud-Aerosol Lidar and Infrared Pathfinder Satellite Observation Observations

Date D/M/Y	CALIPSO overpass time HH:MM UTC[a]	Xuelong latitude (°N)	Xuelong longitude (°E)	Xuelong time HH:MM UTC[a]	Surface visibility (km)	Distance from CALIPSO footprint (km)	CALIPSO VFM cloud-base height (m)
26/08/2016	22:07	73.981	−155.946	22:15	0.207	2.8	0
15/09/2017	22:51	75.630	−171.000	22:30	0.213	2.9	0
12/08/2020	21:36	80.140	−168.860	21:30	0.650	1.4	0
05/08/2016	**16:57**	**80.646**	**−168.422**	**17:30**	**2.25**	**5.0**	**10**
23/09/2017	**23:37**	**64.280**	**−165.700**	**23:30**	**16.2**	**3.1**	**2,590**
30/07/2018	**23:03**	**72.807**	**−167.300**	**22:45**	**11.4**	**0.27**	**1,210**

Note. Bolded text are the collocated events where both CALIPSO and Xuelong did not detect fog.
[a]The local time at the Xuelong location is given by UTC + (Xuelong longitude) ÷ 180 × 12, which is roughly 11 hr preceding the UTC.

2017, and 2020 in which the closest CALIPSO footprint was atmost 30 min and 5 km apart from the closest Xuelong's position (Table 1). The first 3 rows in Table 1 lists are the collocated events where both Xuelong and our CALIPSO detection algorithm reported existence of fog, that is, Xuelong reported a visibility below 1 km and the CALIPSO VFM product indicates zero cloud-base heights.

As an example, Figure 2 shows a visible-band image acquired by the Moderate Resolution Imaging Spectroradiometer on 12 August 2020, around 22:00 UTC (or around 11:00 a.m. local time at near 80°N and 169°W), which shows a large area of reflective clouds around Xuelong (indicated by the red triangle). Figure 3 shows the vertical masks retrieved by CALIPSO along the swath path at 21:36 UTC. The closest CALIPSO footprint along this swath path was only 1.4 km away from Xuelong. The vertical masks show that there was a large layer of ground-touching cloud below 1 km (represented by the cyan shades), indicating sea fog in that area and is consistent with the low visibility of 0.65 km recorded by Xuelong.

The last 3 rows in Table 1 are the collocated events, where Xuelong reported visibility greater than 1 km, implying that no fog was observed during these events according to the WMO definition. Our CALIPSO fog detection algorithm also indicates that the cloud bases during these events were above ground, consistent with the Xuelong records. The collocated event on 6 August 2016 deserves special attention. In this event, the ground-level visibility was 2.25 km. Although it is not classified as a fog event according to the WMO definition, this event is likely a light fog event and we therefore also expect a low cloud-base height. This is supported independently by our CALIPSO fog detection algorithm that returns an estimated cloud-base height of 10 m, which is within the first two vertical layers of CALIPSO.

To sum up, the Xuelong records and our CALIPSO fog detection algorithm are consistent in all six collocated events, three of which had fog and the other three had no fog. Thus, with these six events, the accuracy of CALIPSO detection is 100%, that is, Probability of Detection (POD) = 100% and False Alarm Rate (FAR) = 0%. However, the statistics should not be considered robust for such a small sample size.

3. Results

3.1. Diurnal Variability of Arctic Marine Fog

The visibility sensor on Xuelong operates 24 hr continuously throughout the day, which can be used to estimate the diurnal variability of Arctic marine fog during the summer.

We aggregate all Xuelong 15-min segments collected within the southern half (70°–78°N) and the northern half (78°–86°N) of the selected Chukchi–Beaufort region (defined in Section 2.3) in 1-hr bins and define the fog frequency in a bin as the number of fog events reported, divided by the total number of 15-min segments in the same bin. Thus, the resultant fog frequency is a regional mean in the Chukchi–Beaufort region in the 1-hr bins; the dependence on longitude and latitude will be studied in the next two sections. The number of 15-min segments being used in each 1-hr bin is ~400.

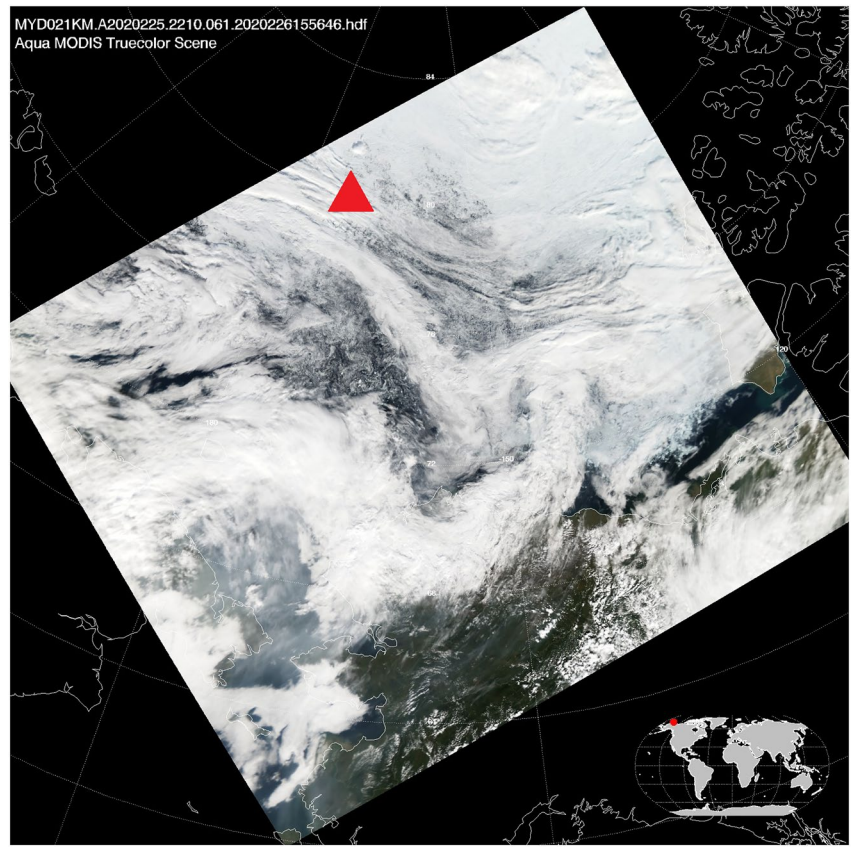

Figure 2. A visible image acquired by Moderate Resolution Imaging Spectroradiometer at 22:10 UTC on 12 August 2020, showing the cloud system near the location of Xuelong (80.140°N, 168.860°W, 21:30 UTC), marked by the red triangle, which was about 6 min before and 1.4 km away from the closest Cloud-Aerosol Lidar and Infrared Pathfinder Satellite Observation overpass. The image was downloaded from https://modis-images.gsfc.nasa.gov/IMAGES/MYD02/GRANULE/granule_frameset_new.html.

The resultant diurnal cycles of the summer marine fog in the southern and northern Chukchi–Beaufort region are shown in Figure 4a. The diurnal cycle variability at 70°–78°N between 6 p.m. and 6 a.m. (next day) stays mostly at ∼12% and has trough of ∼8% between 6 a.m. and 6 p.m. The diurnal cycle at 78°N–86°N show a larger variability. It exhibits a mono-modal structure, where fog is formed most frequently with a maximum probability of ∼18% during the early morning between 1 and 5 a.m., and the fog frequency is mostly below 10% in the rest of the day, with a minimum of ∼3% at noon.

The larger fog frequency diurnal variation in the 78°–86°N latitude band may be related to the relative humidity (Figure 4c). As measured by Xuelong, the relative humidity is higher in the early morning than the rest of the day, favoring the fog formation in the morning. Furthermore, it is closer to saturation at the 78–86°N band at 97.7% than at the lower latitudes due to the lower ambient temperature (Figure 4b).

The diurnal variability discussed above has important implication for interpreting CALIPSO measurements, as we will discuss in Section 3.3.

3.2. Latitudinal Patterns of Arctic Marine Fog

Due to the spatially and temporally limited sampling in the Chukchi–Beaufort seas, it is difficult to obtain a longitude-latitude map of fog frequency using the Xuelong in-situ data. Instead, we average the Xuelong observations over latitude bands to maximize the signal-to-noise ratio of the fog frequency. We aggregate all Xuelong data in 1°-latitude bands defined within the selected Chukchi–Beaufort region and define the fog frequency in a latitude band as the number of fog events reported, divided by the total number of 15-min segments in the same latitude band.

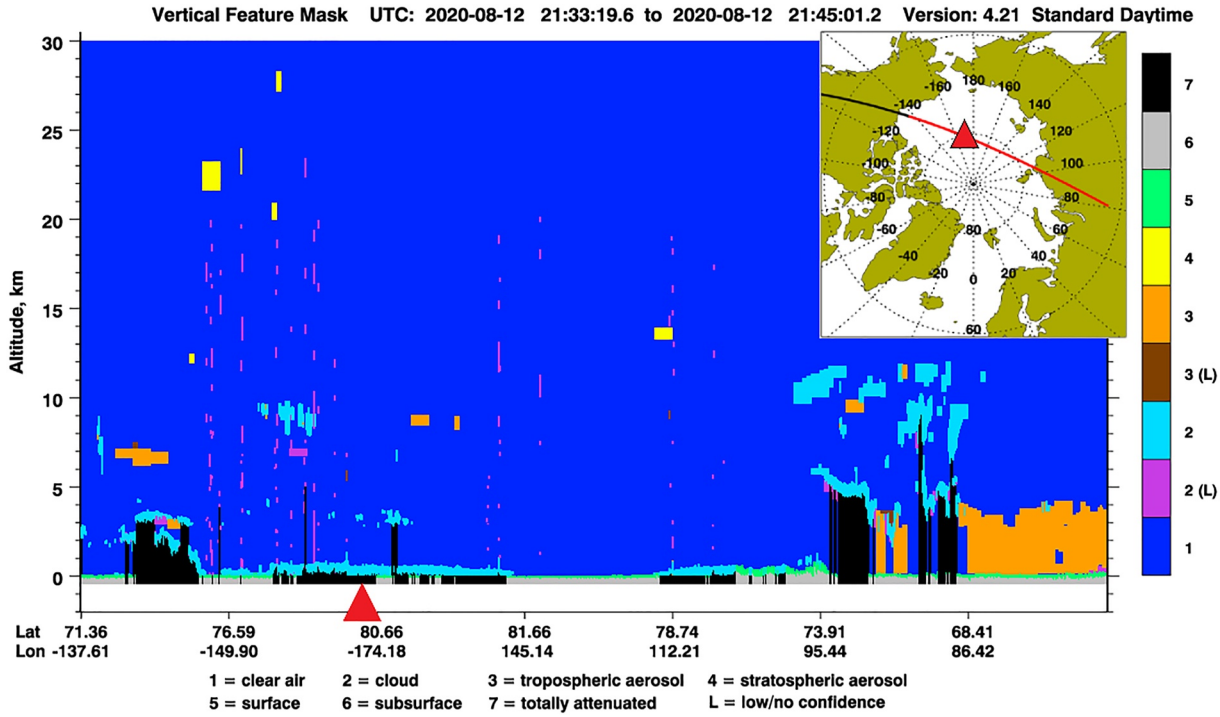

Figure 3. Cloud-Aerosol Lidar and Infrared Pathfinder Satellite Observation Vertical Feature Mask at 21:33 UTC on 12 August 2020. The corresponding segment of the satellite swath path is as a red line shown in the inset. These images have been downloaded from https://www-calipso.larc.nasa.gov/products/lidar/browse_images/std_v4_index.php. The location of Xuelong is indicated by the red triangle. Also see Figure 2 for a visible image of the cloud system at the collocation point.

For comparison with the CALIPSO overpasses in the local mornings, we average the Xuelong in-situ fog frequencies within 2 a.m.–12 p.m. (Figure 5a, blue solid line). It exhibits a rich latitudinal dependence: It has local maxima of ~25% in the latitudinal bands of 72°N–75°N, and 78°N–82°N. The local maxima of the diurnal cycle (Figure 4) are significantly smaller than the local maxima in the latitudinal pattern, likely due to the regional averaging of uneven marine fog distribution. Between the local maxima, the fog frequency is ~5% only. We also obtain a latitudinal average of the Xuelong in-situ fog frequencies within the period 12 p.m.–1 a.m. (Figure 5a, blue dashed line) that was not sampled over the Arctic by CALIPSO. The latitudinal patterns south of 76°N are similar in both time domain. In contrast, the latitudinal patterns north of 76°N have a distinct variability between 78° and 84°N, which leads to the different diurnal variability shown in Figure 4 (green dashed line). We will compare these latitude patterns with that obtained using our CALIPSO detection algorithm in Section 3.3.

The latitudinal pattern of Arctic marine fog is the first of its kind being reported using in-situ visibility measurements but it may be subject to sources of uncertainties including random errors due to the probabilistic nature of fog occurrences, biases in temporal sampling, and biases in spatial sampling. Given that the number of observations used to derive the latitudinal dependence is of the order of 300–1,000 (Figure 5b), the random error is likely less than $\sqrt{\frac{1}{300}}$ or 6% and is much smaller than the maximum fog frequency (~25%). Temporal sampling biases arise because fog occurrence may vary throughout the day in the region (Figure 4), while the vessel may arrive at a certain location at any time during the day. Spatial sampling biases arise because fog formation depends sensitively on regional atmospheric processes, which are affected by, for example, ocean current, sea surface temperature, convergence of warm moist air, landmass and sea ice distributions, etc., but in-situ sampling may not survey the selected region uniformly.

3.3. Longitude-Latitude Patterns of Arctic Marine Fog

To overcome the limitations of the in-situ fog observations, we derive a spatially dense distribution of Arctic summer fog frequency using the CALIPSO VFM product, which provides more uniform coverage of the Arctic up to 82°N at the same local times every day, by aggregating all CALIPSO data in the selected Chukchi–Beaufort region from July to September into 2° × 0.5° grid boxes.

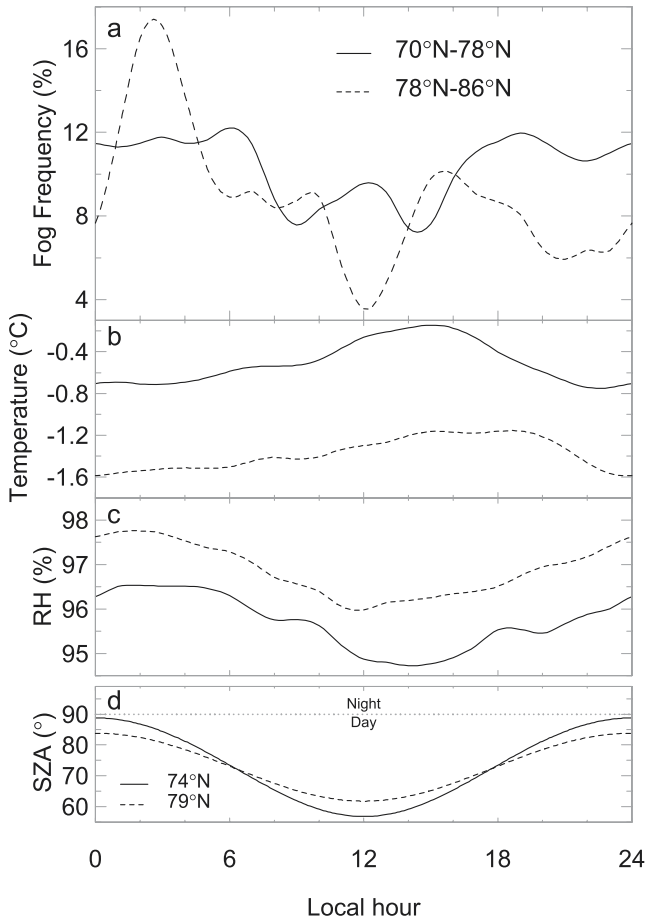

Figure 4. The diurnal cycles of (a) the in-situ fog frequency, (b) ambient temperature, and (c) ambient relative humidity observed aboard Xuelong when the paths were between 176°E and 152°W during the summers (July–September) in 2016, 2017, 2018, and 2020 for two latitude bands: 70°–78°N (solid line) and 78°–86°N (dashed line). (d) Reference solar zenith angle (SZA) at 74° and 79°N, calculated for 1 August 2016 (Hartmann, 1994), indicating the high- and low-sun conditions during the Arctic summer. SZA less than 90° indicates daylight hours.

We note two limitations when using the CALIPSO products. First, the Arctic fog frequency to be obtained using the CALIPSO data are limited only to the morning part of the diurnal cycle due to the sun-synchronous orbit, as explained in Section 2.2. As a result, we expect a higher fog frequency in the CALIPSO-based detection than the diurnally averaged values observed by Xuelong. Second, in a footprint that contains thick clouds, the CALIPSO VFM product may return "no signal" below the lowest vertical cloud layer where the lidar signal below this level is heavily attenuated because of the cloud optical depth being greater than 3, preventing us from detecting fog layers in this footprint. In such cases, we need to ignore the footprint in our fog detection. About 40% of the CALIPSO VFM products in the Chukchi–Beaufort region are ignored in our calculation because of the attenuation. Thus, the CALIPSO-based fog frequency we obtain is an estimate in moderately cloudy scenarios.

The spatial distribution of the CALIPSO-based fog frequency averaged over the 4 summers in 2016, 2017, 2018, and 2020 is shown in Figure 6. There is a band of high fog frequency (24%–36%) extending across the Chukchi Sea around 72°–74°N, which is just north of the entrance to the Bering Strait and is consistent with the largest peak in the Xuelong-based in-situ fog frequency distribution. The fog frequency along coastlines, including the rims of Wrangel Island, is generally lower than the surrounding oceans. There are some weak patches (≤20%) of high fog frequency detected by our CALIPSO detection algorithm at 76°–80°N, which are consistent with the second peak in the Xuelong-based in-situ fog frequency distribution. However, when the spatial distribution is zonally averaged, the CALIPSO fog frequency (shown by the red line in Figure 5a) appears to be a much smoother function of latitudes, having a well-defined peak of ∼20% at 72°N and dropping away from the peak to ∼10% at 70°N (near the entrance of the Bering Strait) and 82°N (the orbital limit). The number of measurements being averaged is on the order of 10^5 after excluding the attenuated footprints. Thus, the second peak of the Xuelong-based in-situ fog frequency distribution at 76°–78°N is not apparent in the zonally averaged CALIPSO-based fog frequency distribution. We also compute the CALIPSO-based fog frequency distribution in individual summers and we find that the smoothness of the CALIPSO-based fog frequency distribution remains robust in time.

The linear Pearson correlation coefficient of fog frequency from our CALIPSO detection algorithm (red line) and Xuelong observations (blue line) in Figure 5a from 70.5° to 82°N (24 grid points at 0.5° resolution) is higher than 0.59 (99% confidence).

4. Discussions and Concluding Remarks

Our analysis demonstrates that in-situ Xuelong and spaceborne CALIPSO observations of Arctic marine fog in the Chukchi–Beaufort region of the Pacific Arctic complement each other's shortcomings in spatial and temporal samplings. A combination of these observations helps reveal rich spatiotemporal variability of fog frequency distribution.

The in-situ Xuelong observations show that the fog frequency in the northern Chukchi–Beaufort region is ∼18% in the early morning (1–5 a.m.) and is at least 2 times of the fog frequency in the rest of the day. This modal diurnal variability of marine fog is similar to the diurnal variability of low-lying cloud (cloud-base height below 2 km) observed over the Barrow observatory during the "day" regime reported in Shupe et al. (2011), where both exhibit a maximum fog frequency in the early morning. However, the diurnal variability observed by Xuelong is significantly different from that observed by SHEBA, although both measurements were performed

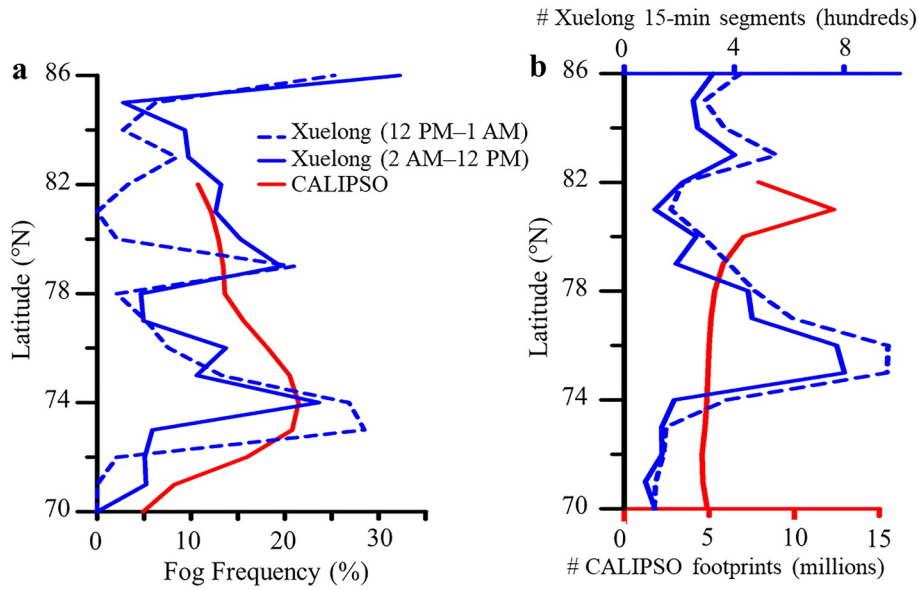

Figure 5. (a) The zonal average of fog frequency between 176°E and 152°W based on our Cloud-Aerosol Lidar and Infrared Pathfinder Satellite Observation (CALIPSO) detection algorithm (red) and Xuelong in-situ observations (blue). (b) The number of CALIPSO- (red) and Xuelong-based (blue) observations being averaged in Panel (a). The northmost latitude of Xuelong reached was 86°N, while that of the CALIPSO's sun-synchronous orbit is 82°N.

in the Beaufort Sea. Since SHEBA drifted with permanent ice packs in the Beaufort Sea, the difference between SHEBA and Xuelong may indicate different low-lying cloud structures over sea ice and open water. The latitudinal distribution of the Xuelong-based fog frequency further reveals the peaks of fog occurrences at 74° and 79°N.

The longitude-latitude distribution of fog frequency derived using our CALIPSO fog detection algorithm shows a few local regions of high fog occurrences near 72°–74°N and 76°–80°N in the central Chukchi–Beaufort region that are consistent with the latitudinal distribution of the Xuelong-based fog frequency sampled between 2 a.m. and 12 p.m. Thus, although the CALIPSO-based fog frequency is limited to moderately cloudy scenarios (i.e., optical depth ≥3), the qualitative agreement between the Xuelong-based and CALIPSO-based fog frequency suggests that the fog frequency distribution in the Chukchi–Beaufort region may be similar in different cloudiness conditions.

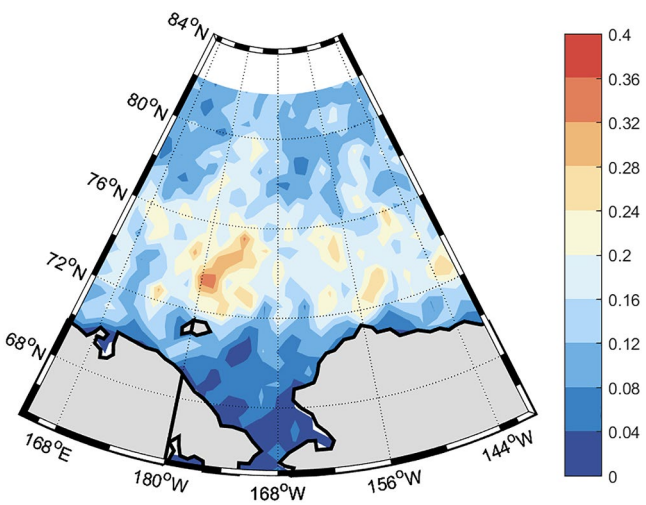

Figure 6. The longitude-latitude distribution of the marine fog frequency in the Chukchi-Beaufort region derived using the Vertical Feature Masks product of Cloud-Aerosol Lidar and Infrared Pathfinder Satellite Observation. The distribution is an average over the summers (July–September) of 2016, 2017, 2018, and 2020.

In addition, we note that the longitude-latitude distribution of the CALIPSO-based fog frequency is lower along the continental coastlines than over remote ocean regions. This longitude-latitude distribution informs the role of atmospheric processes involved in the Arctic marine fog formation. During the Arctic summer (July–September), the inflow into the Pacific Arctic through the Bering Strait is ~1 Sv and the inflow temperature is ~2°C (Timmermans & Marshall, 2020; Woodgate et al., 2005). The clockwise circulation in the Beaufort Gyre forces the warm inflow to travel northward along the coastlines of Alaska and Siberia. Although the inflow provides moisture into the Arctic region, the warmth brought in by the inflow suppresses the formation of inverse layers, leading to the low fog frequencies along the coastlines. In contrast, the Beaufort Gyre north of Alaska mixes cold Arctic waters from deep polar region southward, favoring the formation of inversion layers for fog formation during frontogenesis where the cold front from the deep Arctic meets with the warm inflow from the Pacific. In addition, sea ice formed within the Beaufort Gyre in the previous winter also provide dry and cold environment favoring fog formation. Thus, fog is more

likely to form at the southern rims of the Beaufort Gyre, consistent with Figure 6, which shows the highest fog frequency in regions near the Bering Strait entrance.

We have shown that the climatological averages of Xuelong- and CALIPSO-based fog frequencies presented above agree well with each other. In addition, the six collocated Xuelong and CALIPSO events also agree well, giving a POD of 100% and an FAR of 0%. The 0% FAR implies that our CALIPSO detection algorithm has 100% confidence in a detected fog event. Thus, from a captain's perspective, if our CALIPSO detection algorithm reports fog on the route, the safest decision is to either postpone the voyage (although a financial loss to the shipping company is incurred) or revise the voyage plan with a detour around the region where fog is detected. The high POD and the low FAR of our CALIPSO detection algorithm thus help improve the confidence of the fog alert system, and reduce the accident rates and the costs of navigation in the Pacific Arctic region.

Data Availability Statement

CALIPSO products were downloaded from https://www-calipso.larc.nasa.gov/tools/data_avail/. The Xuelong in-situ data used in this study can be obtained from Dryad https://doi.org/10.6086/D1P40N.

Acknowledgments
YL was supported by the National Key Research and Development Program of China (2019YFA0607000), the National Natural Science Foundation of China (41975024). KFL and KKT were supported by the Belmont Forum and the U.S. National Science Foundation through Grant NSF1536175, and by National Aeronautics and Space Administration through Grant NNX14AR40G. XC was supported by the Belmont Forum and the Natural Science Foundation of China through Grant 41561144001, the National Key Research and Development Program of China under Grants by 2019YFA0607000, and Basic Science foundation of Ocean University of China under Grant 202071001. We thank the crew of Chinese R/V Xuelong I and II for their assistance during our study.

References

Andreas, E. L. (2004). Spray stress revisited. *Journal of Physical Oceanography*, *34*(6), 1429–1440. https://doi.org/10.1175/1520-0485(2004)034<1429:SSR>2.0.CO;2

Dorman, C. E., Mejia, J., Koračin, D., & McEvoy, D. (2017). Worldwide marine fog occurrence and climatology. In D. Koračin & C. E. Dorman (Eds.), *Marine fog: Challenges and advancements in observations, modeling, and forecasting* (pp. 7–152). Springer International Publishing.

Eastman, R. M., & Warren, S. G. (2010). Interannual variations of Arctic cloud types in relation to sea ice. *Journal of Climate*, *23*(15), 4216–4232. https://doi.org/10.1175/2010JCLI3492.1

Hartmann, D. L. (1994). *Global physical climatology*. Academic Press.

Intrieri, J. M., Fairall, C. W., Shupe, M. D., Persson, P. O. G., Andreas, E. L., Guest, P. S., & Moritz, R. E. (2002). An annual cycle of Arctic surface cloud forcing at SHEBA. *Journal of Geophysical Research*, *107*(C10), 8039. https://doi.org/10.1029/2000JC000439

Kay, J. E., & Gettelman, A. (2009). Cloud influence on and response to seasonal Arctic sea ice loss. *Journal of Geophysical Research*, *114*(D18), D18204. https://doi.org/10.1029/2009JD011773

Koračin, D., Dorman, C. E., Lewis, J. M., Hudson, J. G., Wilcox, E. M., & Torregrosa, A. (2014). Marine fog: A review. *Atmospheric Research*, *143*, 142–175. https://doi.org/10.1016/j.atmosres.2013.12.012

Mülmenstädt, J., Sourdeval, O., Henderson, D. S., L'Ecuyer, T. S., Unglaub, C., Jungandreas, L., et al. (2018). Using CALIOP to estimate cloud-field base height and its uncertainty: The Cloud Base Altitude Spatial Extrapolator (CBASE) algorithm and dataset. *Earth System Science Data*, *10*(4), 2279–2293. https://doi.org/10.5194/essd-10-2279-2018

Naval Weather Service. (1978). *Study of worldwide occurrence of fog, thunderstorms, supercooled low clouds and freezing temperatures, NAVAIR 50-IC-60 CH-I*. Naval Oceanography and Meteorology.

Palm, S. P., Strey, S. T., Spinhirne, J., & Markus, T. (2010). Influence of Arctic sea ice extent on polar cloud fraction and vertical structure and implications for regional climate. *Journal of Geophysical Research*, *115*(D21), D21209. https://doi.org/10.1029/2010JD013900

Schweiger, A. J., Lindsay, R. W., Vavrus, S., & Francis, J. A. (2008). Relationships between Arctic sea ice and clouds during autumn. *Journal of Climate*, *21*(18), 4799–4810. https://doi.org/10.1175/2008JCLI2156.1

Shupe, M. D., Walden, V. P., Eloranta, E., Uttal, T., Campbell, J. R., Starkweather, S. M., & Shiobara, M. (2011). Clouds at Arctic atmospheric observatories. Part I: Occurrence and macrophysical properties. *Journal of Applied Meteorology and Climatology*, *50*(3), 626–644. https://doi.org/10.1175/2010JAMC2467.1

Smith, L. C., & Stephenson, S. R. (2013). New Trans-Arctic shipping routes navigable by midcentury. *Proceedings of the National Academy of Sciences*, *110*(13), E1191–E1195. https://doi.org/10.1073/pnas.1214212110

Snape, T. J., & Forster, P. M. (2014). Decline of Arctic sea ice: Evaluation and weighting of CMIP5 projections. *Journal of Geophysical Research: Atmospheres*, *119*(2), 546–554. https://doi.org/10.1002/2013JD020593

Timmermans, M. L., & Marshall, J. (2020). Understanding Arctic Ocean circulation: A review of Ocean dynamics in a changing climate. *Journal of Geophysical Research: Oceans*, *125*(4), e2018JC014378. https://doi.org/10.1029/2018JC014378

Uttal, T., Curry, J. A., McPhee, M. G., Perovich, D. K., Moritz, R. E., Maslanik, J. A., et al. (2002). Surface heat budget of the Arctic Ocean. *Bulletin America Meteorology Social*, *83*(2), 255–275. https://doi.org/10.1175/1520-0477(2002)083<0255:SHBOTA>2.3.CO;2

Venne, M. G., Jasperson, W. H., & Venne, D. E. (1997). *Difficult weather: A review of thunderstorm, fog and stratus, and winter precipitation forecasting*. Air Force Materiel Command.

Wang, X., & Key, J. R. (2005). Arctic surface, cloud, and radiation properties based on the AVHRR Polar Pathfinder dataset. Part II: Recent trends. *Journal of Climate*, *18*(14), 2575–2593. https://doi.org/10.1175/JCLI3439.1

Winker, D. M., Hunt, W. H., & McGill, M. J. (2007). Initial performance assessment of CALIOP. *Geophysical Research Letters*, *34*(19), L19803. https://doi.org/10.1029/2007GL030135

Winker, D. M., Vaughan, M. A., Omar, A., Hu, Y., Powell, K. A., Liu, Z., et al. (2009). Overview of the CALIPSO mission and CALIOP data processing algorithms. *Journal of Atmospheric and Oceanic Technology*, *26*(11), 2310–2323. https://doi.org/10.1175/2009JTECHA1281.1

WMO. (2005). *Aerodrome reports and forecasts: A user's handbook to the codes* (4th ed.). World Meteorological Organization.

Woodgate, R. A., Aagaard, K., & Weingartner, T. J. (2005). Monthly temperature, salinity, and transport variability of the Bering Strait through flow. *Geophysical Research Letters*, *32*(4), L04601. https://doi.org/10.1029/2004GL021880

Wu, D., Lu, B., Zhang, T., & Yan, F. (2015). A method of detecting sea fogs using CALIOP data and its application to improve MODIS-based sea fog detection. *Journal of Quantitative Spectroscopy and Radiative Transfer*, *153*, 88–94. https://doi.org/10.1016/j.jqsrt.2014.09.021

Yi, L., Li, K.-F., Chen, X., & Tung, K.-K. (2019). Arctic fog detection using infrared spectral measurements. *Journal of Atmospheric and Oceanic Technology*, *36*(8), 1643–1656. https://doi.org/10.1175/jtech-d-18-0100.1